driving force for reaction 2, this result is in reasonable agreement with the findings of Guarr and McLendon which indicate that the thermal reactions between $Ru(bpy)_3^{3+}$ and homologues of methyl viologen, having driving forces of 0.1 to 0.6 V, require a mean separation between the reactants ranging from a contact distance to 10 Å in glycerol at 0 °C.[93]

## Conclusion

These data indicate that disproportionation on PVG occurs via a reaction sequence very similar to that which occurs in aqueous solution.[40] Biphotonic excitation photoionizes the complex and the photodetached electron reduces a second $Ru(bpy)_3^{2+}$ ion. In aqueous solution, product lifetime is limited by the thermal back reaction which occurs because the products are free to diffuse about the reaction medium. On this support, however, the reactants are fixed, whereas the photodetached electron, after thermal excitation from initially populated surface sites, is a mobile intermediate. Consequently, disproportionation only occurs when the mean separation between the reacting adsorbate ions is within the electron migration distance. On the other hand, the electron migration distance, which these and other experiments indicate is on the order of 50 Å[46,81,92] exceeds the mean separation, ≤13 Å, necessary for the thermal back reaction, and the reaction products are stable. Increasing the amount adsorbed increases the probability of the thermal back reaction by decreasing the mean product separation, and the quantum efficiency of the reaction declines.

This apparent "photochemical diode" effect[32] appears to arise from two factors on this support. First is the availability of electron acceptors sites on the surface. These are thought to be shallow energy wells from which the electron can be thermally activated but, nevertheless, present an energy barrier, albeit slight, which prevents immediate recombination. Energetically, they perform a function similar to band bending which promotes charge separation on the more conventional metal oxide semiconductors.[94] Second is that the electron migration distance exceeds that necessary for the thermal back reaction.

**Acknowledgment.** Support of this research by the Research Foundation of the City University of New York, the Dow Chemical Co.'s Technology Acquisition Program, and the donors of the Petroleum Research Fund, administered by the American Chemical Society, is gratefully acknowledged. H.D.G. and M.B. thank the Andrew W. Mellon Foundation for Fellowships during 1982-1983, and Dr. David L. Morse of the Corning Glass Co. for samples of porous Vycor glass.

(93) Guarr, T.; McLendon, C., Abstracts, 182nd National Meeting of the American Chemical Society, New York, 1981: INORG 20.

(94) Novak, A. J., "Photochemical Conversion and Storage of Solar Energy"; Connolly, J. S., Ed.; Academic Press: New York, 1981; p 271.

# CO Activation by Biscyclopentadienyl Complexes of Group 4 Metals and Actinides: $\eta^2$-Acyl Complexes[⊥]

**Kazuyuki Tatsumi,*[†] Akira Nakamura,[†] Peter Hofmann,*[‡] Peter Stauffert,[‡] and Roald Hoffmann*[§]**

*Contribution from the Department of Macromolecular Science, Faculty of Science, Osaka University, Toyonaka, Osaka 560, Japan, Anorganisch-chemisches Institut der Technischen Universität München, D-8046 Garching, Federal Republic of Germany, and Department of Chemistry, Cornell University, Ithaca, New York 14853.* *Received October 9, 1984*

**Abstract:** The electronic and geometrical structure and reactivity of $\eta^2$-acyl complexes of group 4 transition metals and of actinides are the subject of this paper. The directionality of the LUMO of $d^0$ $Cp_2MI_2$ systems favors a lateral or outside approach of a CO over a central one. Next the electronic structures of the $\eta^2$ acyls themselves are analyzed, and overlap reasons given for the preference for $\eta^2$ coordination in the Ti, Zr, and actinide complexes that are the main subject of this study, in contrast to the $\eta^1$ coordination in 18-electron Mn acyls. Our potential energy surfaces and qualitative analysis point to a preference for the O-inside $\eta^2$-acyl conformer for Ti and Zr, and approximately equal energies for O-inside and O-outside conformers for U and Th. We also find an unexpected $\eta^1$ minimum in the O-outside surfaces, with an orbital symmetry imposed barrier to slipping to the $\eta^2$ minimum. This suggests a pathway for the interconversion of the O-outside and O-inside $\eta^2$ isomers through an as yet unobserved $\eta^1$ structure. Separate oxycarbene isomers are also located, but these are at high energy. We believe the electrophilic reactivity of the $\eta^2$ acyls does not depend on reaching the oxycarbene isomers, but may be traced to a low-lying carbenium-ion-like acceptor orbital in the undistorted $\eta^2$-acyl structure.

## Introduction

A particularly fascinating aspect of the activation of carbon monoxide by transition metal compounds is the carbonylation chemistry of biscyclopentadienyl dialkyls (diaryls), haloalkyls, and related derivatives of group 4 d metals[1] and of actinides,[2,3] $Cp_2MR_2$ and $Cp_2MRX$. CO insertion processes into the M-R bonds of these complexes are extremely facile and while not catalytic have served as models for the CO activation and reductive CO coupling steps of some potentially industrially important catalytic processes.[4]

[⊥] In this paper the periodic group notation is in accord with recent actions by IUPAC and ACS nomenclature committees. A and B notation is eliminated because of wide confusion. Groups IA and IIA become groups 1 and 2. The d-transition elements comprise groups 3 through 12, and the p-block elements comprise groups 13 and 18. (Note that the former Roman number designation is preserved in the last digit of the new numbering: e.g., III→3 and 13.)

[†] Osaka University.

[‡] Anorganisch-chemisches Institut der Technischen Universität München.

[§] Cornell University.

(1) (a) Fachinetti, G.; Floriani, C.; Marchetti, F.; Merlino, S. *J. Chem. Soc., Chem. Commun.* **1976**, 522-523. (b) Fachinetti, G.; Fochi, G.; Floriani, C. *J. Chem. Soc., Dalton Trans.* **1977**, 1946-1950. (c) Manriquez, J. M.; McAlister, D. R.; Sanner, R. D.; Bercaw, J. E. *J. Am. Chem. Soc.* **1976**, *98*, 6733-6735; **1978**, *100*, 2716-2724. (d) Wolczanski, P. T.; Bercaw, J. E. *Acc. Chem. Res.* **1980**, *13*, 121-127. (e) Erker, G. *Ibid.* **1984**, *17*, 103-109, and references therein. (f) Calderazzo, F. *Angew. Chem.* **1977**, *89*, 305-317. (g) Marsella, J. A.; Moloy, K. G.; Caulton, K. G. *J. Organomet. Chem.* **1980**, *201*, 389-398. (h) Baldwin, J. C.; Keder, N. L.; Strouse, C. E.; Kaska, W. C. *Z. Naturforsch.* **1980**, *35b*, 1289-1297. (i) Jeffery, J.; Lappert, M. F.; Luong-Thi, M. T.; Webb, M. *J. Chem. Soc., Dalton Trans.* **1981**, 1593-1605. (j) Bristow, G. S.; Hitchcock, P. B.; Lappert, M. F. *J. Chem. Soc., Chem. Commun.* **1982**, 462-464. (k) Klei, E.; Teuben, J. H. *J. Organomet. Chem.* **1981**, *222*, 79-88. (l) For some related isocyanide chemistry, see: Wolczanski, P. T.; Bercaw, J. E. *J. Am. Chem. Soc.* **1979**, *101*, 6450-6452.

0002-7863/85/1507-4440$01.50/0 

The isolable CO insertion products of biscyclopentadienyl complexes of group 4 metals and of actinides have revealed some unusual structural features. They contain acyl groups, RCO, that have both carbon and oxygen atoms bound to the same transition metal center.[5,6] This $\eta^2$ coordination mode has an interesting aspect, namely, that there are two possible isomers, one with the C–O vector pointing away from the additional ligand X (**1**) and

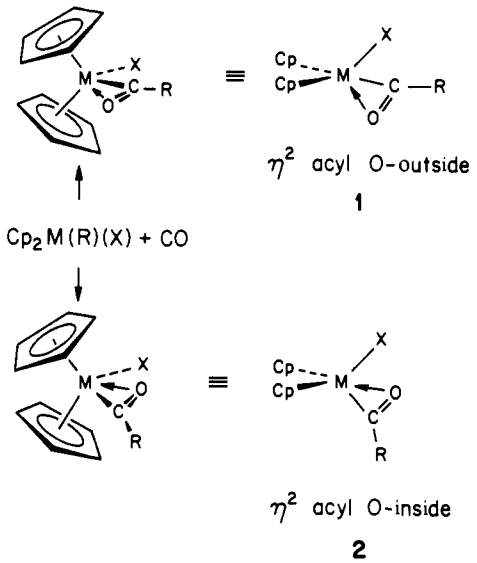


the other one with the opposite C–O orientation (**2**). Acyl complexes of group 4 metals, such as $Cp_2Ti(COCH_3)Cl$[5] and $Cp_2Zr(COCH_3)(CH_3)$,[1a,b] show structures of type **2**. In contrast, the actinide analogues favor structure **1**, or at least **1** can be as stable as **2**. Thus the acyl ligand of $Cp_2$*Th[$COCH_2C(CH_3)_3$]Cl[7] orients as **1**, while in the related carbamoyl compounds $Cp_2$*Th($CONR_2$)Cl and $Cp_2$*U($CONR_2$)Cl,[8a] both conformers are in equilibrium. $Cp_2$*Th($\eta^2$-$COC_6H_5$)Cl has the $\eta^2$ O-inside structure, **2**.[8b] Furthermore, the biscyclopentadienyl actinides ($Cp_2$*An) accomodate as many as two $\eta^2$ carbamoyl ligands,[8] **3**.

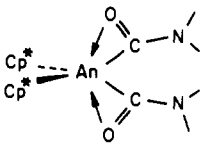

**3**

These are formally 20-electron compounds and a group 4 metal complex of this type is unlikely to be stable.

The recent mechanistic study of the carbonylation of $Cp_2ZrR_2$ enables us to view the geometrical choice between **1** and **2** in a more profound way.[9] The O-inside conformer **2**, as found in the X-ray analysis of the acyl compound, is not the initial kinetic product. Instead, CO insertion into the Zr–R bond seems to yield an intermediate, very possibly of structure **1**, which subsequently isomerizes irreversibly to its thermodynamically more stable form **2**.

Another interesting point to be mentioned here is the reactivity of such $\eta^2$-acyl biscyclopentadienyl complexes, e.g., reactions with nucleophiles such as metal halides,[10-12] acyl to ketene or ketenimine transformations,[13-15] ketone ligand formation,[16,17] deprotonation of the acyl ligands,[14] and reductive CO coupling.[18] These features have often been attributed to the "oxycarbene" character of $\eta^2$-acyl ligands, invoking a resonance structure **4b** which is thought to contribute to the bonding in addition to the $\eta^2$-acyl structure **4a**.

The observed C–O stretching frequencies ($\nu_{CO}$) of $\eta^2$ acyls may provide an argument in favor of the contribution of **4b**. Typical $\nu_{CO}$'s for transition metal $\eta^1$ acyls range from 1630 to 1680 $cm^{-1}$, while those for $\eta^2$ acyls are in the range ~1530–1620 $cm^{-1}$. The decrease in $\nu_{CO}$ on forming $\eta^2$ acyl is significant in the case of $Cp_2$*Th(COR)X and $Cp_2$*Th(COR)R', ($\nu_{CO}$ ~1450–1480 $cm^{-1}$).[2a,h] However, in the X-ray structures of $Cp_2Ti(COCH_3)Cl$,[5] $Cp_2Zr(COCH_3)(CH_3)$,[1b] and $Cp_2$*Th($COCH_2$'Bu)Cl,[7] the C–O distances are not elongated as much as one might expect from the resonance form **4b**. There remain some doubts about significant participation of resonance form **4b** in the ground-state

(2) (a) Marks, T. J.; Manriquez, J. M.; Fagan, P. J.; Day, V. W.; Day, C. S.; Vollmer, S. H. *ACS Symp. Ser.* **1980**, *No. 131*, 1–29. (b) Fagan, P. J.; Maatta, E. A.; Marks, T. J. *Ibid.* **1981**, 152, 52–78. (c) Marks, T. J. *Science* **1982**, *217*, 989–997. (d) Marks, T. J. *Prog. Inorg. Chem.* **1979**, *25*, 224–333. (e) Manriquez, J. M.; Fagan, P. J.; Marks, T. J.; Day, C. S.; Day, V. W. *J. Am. Chem. Soc.* **1978**, *100*, 7112–7114. (f) Fagan, P. J.; Moloy, K. G.; Marks, T. J. *Ibid.* **1981**, *103*, 6959–6962. (g) Maatta, E. A.; Marks, T. J. *Ibid.* **1981**, *103*, 3576–3578. (h) Moloy, K. G.; Marks, T. J. *Ibid.* **1984**, *106*, 7051–7064.

(3) (a) Intriguing is a CO insertion into the U=C double bond in $Cp_3UCHP(CH_3)(C_6H_5)_2$, which leads to the $\eta^2$ $\beta$-keto ylide structure: Cramer, R. E.; Maynard, R. B.; Paw, J. C.; Gilje, J. W. *Organometallics* **1982**, *1*, 869–871. (b) A coordinated carbonyl in $CpMn(CO)_3$ or $[CpFe(CO)_2]_2$ can also be inserted into the U=C bond in $Cp_3U$ CHP-$(CH_3)(C_6H_5)(R)$ (R = $CH_3$, $C_6H_5$): Cramer, R. E.; Higa, K. T.; Gilje, J. W. *J. Am. Chem. Soc.* **1984**, *106*, 7245–7247. (c) Remarkably facile CO insertion into M–C and M–N bonds (M = Th, U) were also found for $Cp_3ThR$, $Cp_3UR$, and $Cp_3UNR_2$: Sonnenberger, D. C.; Mintz, E. A.; Marks, T. J. *Ibid.* **1984**, *106*, 3484–3491. Paolucci, G.; Rossetto, G.; Zanella, P.; Yünlü, K.; Fischer, R. D., *J. Organomet. Chem.* **1984**, *272*, 363–383. (d) Insertions of isocyanides into the U–C bonds of $Cp_3UR$, $Cp^*_2URCl$, and $Cp^*_2UR_2$ have recently appeared: Dormond, A.; Elbouadili, A. A.; Moise, C. *J. Chem. Soc., Chem. Commun.* **1984**, 749–751. Zanella, P.; Paolucci, G.; Rossetto, G.; Benetollo, F.; Polo, A.; Fischer, R. D.; Bombieri, G. *Ibid.* **1985**, 96–98.

(4) For general aspects of CO insertion reactions, see, for example: Collman, J. P.; Hegedus, L. S. "Principles and Applications of Organotransition Metal Chemistry"; University Science Books: Mill Valley, CA, 1980. See also ref 1f.

(5) $Cp_2Ti(COCH_3)Cl$ was formed by the reaction between $Cp_2Ti(CO)_2$ and $CH_3COCl$: Fachinetti, G.; Floriani, C.; Stöckli-Evans, H. *J. Chem. Soc., Dalton Trans.* **1977**, 2297–2302.

(6) Several examples of $\eta^2$-acyl groups bridging two metal centers are known: (a) Mott, G. N.; Grauby, R.; MacLaughlin, S. A.; Tailor, N. J.; Carty, A. J. *Organometallics* **1983**, *2*, 189–191. (b) Longato, B.; Norton, J. R.; Huffman, J. C.; Marsella, J. A.; Caulton, K. G. *J. Am. Chem. Soc.* **1981**, *103*, 209–210; **1982**, *104*, 6360–6368. (c) Jeffery, J. C.; Orpen, A. G.; Robinson, W. T.; Stone, F. G. A.; Went, M. J. *J. Chem. Soc., Chem. Commun.* **1984**, 396–398. (d) Henrick, K.; Iggo, J. A.; Mays, M. J.; Raithby, P. R. *Ibid.* **1984**, 209–211. (e) Szostak, R.; Strouze, C. E.; Kaesz, H. D. *J. Organomet. Chem.* **1980**, *191*, 243–260. (f) Johnson, B. F. G.; Lewis, J.; Odiaka, T. I.; Raithby, P. R. *Ibid.* **1981**, *216*, C56–C60. (g) LaCroce, S. J.; Cuttler, A. R. *J. Am. Chem. Soc.* **1982**, *104*, 2312–2314, and references therein.

(7) Fagan, P. J.; Manriquez, J. M.; Marks, T. J.; Day, V. W.; Vollmer, S. H.; Day, C. S. *J. Am. Chem. Soc.* **1980**, *102*, 5393–5396.

(8) (a) Fagan, P. J.; Manriquez, J. M.; Vollmer, S. H.; Day, C. S.; Day, V. W.; Marks, T. J. *J. Am. Chem. Soc.* **1981**, *103*, 2206–2220. (b) Marks, T. J., private communication.

(9) (a) Erker, G.; Rosenfeldt, F. *Angew. Chem., Int. Ed. Engl.* **1978**, *17*, 605–606. (b) Erker, G.; Rosenfeldt, F. *J. Organomet. Chem.* **1980**, *188*, C1–C4.

(10) Threlkel, R. H.; Bercaw, J. E. *J. Am. Chem. Soc.* **1981**, *103*, 2650–2659.

(11) Gell, K. I.; Posin, P.; Schwartz, J.; Williams, G. M. *J. Am. Chem. Soc.* **1982**, *104*, 1846–1855.

(12) (a) Marsella, J. A.; Folting, K.; Huffman, J. C.; Caulton, K. G. *J. Am. Chem. Soc.* **1982**, *103*, 5596–5598. (b) Marsella, J. A.; Huffman, J. C.; Caulton, K. G.; Longato, B.; Norton, J. R. *Ibid.* **1982**, *104*, 6360–6368.

(13) Complexed $Ph_2C$=C=O is formed in carbonylations of zirconocene dialkyls; see ref 1j.

(14) (a) Straus, D. A.; Grubbs, R. H. *J. Am. Chem. Soc.* **1982**, *104*, 5499–5500. (b) Moore, E. J.; Straus, D. A.; Armantrout, J.; Santarsiero, B. D.; Grubbs, R. H.; Bercaw, J. E. *Ibid.* **1983**, *105*, 2068–2070. (c) Ho, D. S. C.; Straus, D. A.; Armantrout, J.; Schaefer, W. P.; Grubbs, R. H. *Ibid.* **1984**, *106*, 2210–2111.

(15) Moloy, K. G.; Marks, T. J.; Day, V. W. *J. Am. Chem. Soc.* **1983**, *105*, 5696–5698.

(16) (a) Rosenfeldt, F.; Erker, G. *Tetrahedron Lett.* **1980**, 1637–1640. (b) Erker, G.; Rosenfeldt, F. *J. Organomet. Chem.* **1982**, *224*, 29–42. (c) Erker, G.; Kropp, K. *Chem. Ber.* **1982**, *115*, 2437–2446.

(17) Related is the formaldehyde ligand formation, e.g., from $Cp_2ZrHCl$ and CO: (a) Gambarotta, S.; Floriani, C.; Chiesi-Villa, A.; Guastini, C. *J. Am. Chem. Soc.* **1983**, *105*, 1690–1691. (b) Erker, G.; Kropp, K.; Krüger, C.; Chiang, A. P. *Chem. Ber.* **1982**, *115*, 2447–2460.

(18) See, for example, ref 1d, 1e, and 2a. $Cp_2Zr(CH_3)_2$ under appropriate conditions also undergoes the CO coupling reaction: Erker, G., private communication. Rosenfeldt, F. Ph.D. Thesis, Universität Bochum, 1981.

structures of these acyl complexes. Or it may be that there is

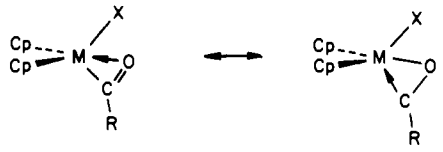

4a 4b

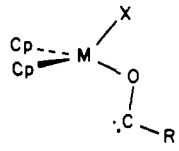

5

yet another metastable structure of an oxycarbene isomer **5**, from which the carbene-type reactions could proceed.

### CO Insertion Process

Lauher and Hoffmann have predicted that the initial attack of CO on $d^0$ $Cp_2MR_2$ (M = Ti and Zr) occurs along the line perpendicular to the Cp centroid–metal–Cp centroid plane, as marked by A in **6**.[19] This favorable approach was anticipated

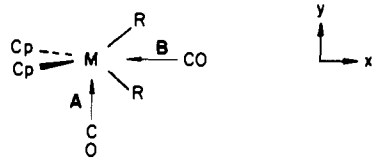

6

from the spatial extention of the LUMO of $d^0$ $Cp_2ML_2$, approximately of a "$y^2$" type, **7a**. The shape of the LUMO should allow for better overlap with the carbon lone pair (HOMO), **7b**, through a "lateral" approach A compared with the alternative "central" pathway B. Note that the coordinate system chosen for $Cp_2ML_2$ complexes in **6** and throughout this paper is different from the one defined in the paper by Lauher and Hoffmann.[19] In ref 19, the choice is tied to $C_{2v}$ symmetry, with $z$ along the twofold axis instead of $x$.

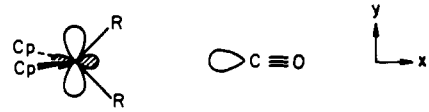

LUMO HOMO

7a 7b

Let us begin our theoretical analysis with a study of the CO insertion processes of the model molecules $Cp_2Zr(CH_3)_2$ and $Cp_2U(CH_3)_2^{2+}$. Since the extended Hückel method is not very well suited for describing energetics of bond-breaking and bond-formation steps, we examine the initial stages of a CO attack. The calculations were performed by varying the carbon (CO)-to-metal distance, $L$, from 4.5 to 3.0 Å for $Cp_2Zr(CH_3)_2$ + CO and from 5.0 to 3.5 Å for $Cp_2U(CH_3)_2^{2+}$ + CO. The uranium complex with 2+ charge has a $5f^0$ $6d^0$ electronic configuration and corresponds to $Cp_2Th(CH_3)_2$.[20] At each point along the central attack pathway B, the $CH_3$–M–$CH_3$ angle was optimized, while the geometry of the $Cp_2M$ fragment was kept fixed. $C_{2v}$ molecular symmetry was preserved throughout the association path. For the lateral approach A, we independently optimized

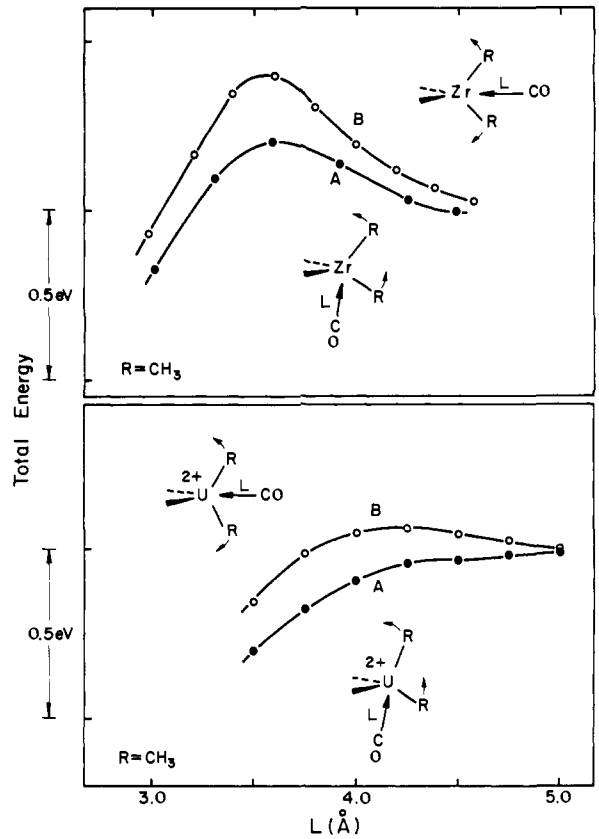


**Figure 1.** Total energy profiles for the two CO approaches toward $Cp_2Zr(CH_3)_2$ (top) and $Cp_2U(CH_3)_2^{2+}$ (bottom). The curves connecting filled circles are for a "lateral" approach A and those connecting open circles are for a "central" approach B.

the angular positions of all three ligands, two $CH_3$ groups and CO, thereby allowing for the best ligand arrangement within the $xy$ plane as CO approaches.

Figure 1, top, gives the total energy curves for the CO attack on $Cp_2Zr(CH_3)_2$ as a function of the Zr–CO distance $L$. It is found that the lateral pathway A, accompanied by an appropriate relaxation of the methyl positions, is energetically favored. The result confirms that a CO molecule will indeed keep out of the central route B as Lauher and Hoffmann had suggested. The two curves for the Zr system go through a small barrier at about $L$ = 3.5 Å. This is the region where closed-shell–closed-shell repulsions still outweigh the attractive interaction between the HOMO **7b** and the LUMO **7a**. Pathway A is characterized by stronger HOMO–LUMO bonding interaction, due to the better overlap. Therefore, the calculated activation energy of pathway A is smaller by about 0.2 eV (~5 kcal/mol) than that of pathway B. The difference is not that much, but we think it will easily suffice to induce regiospecificity for the primary CO attack.[21] On the left side of Figure 1, top the energy drops. In this connection we note that reaction enthalpies of −12.7 and −11.7 kcal/mol have been found for CO insertion into the Hf–R bond of $Cp_2HfR_2$ (R = $CH_3$ and $CH_2C_6H_5$).[1b]

The potential energy curves for the two pathways of carbonylation of $Cp_2U(CH_3)_2^{2+}$ are shown in Figure 1, bottom. Again the lateral pathway A is slightly preferred. Our calculations give a barrier of 0.1 eV (~2 kcal/mol) for B, while attack along A does not encounter an appreciable barrier. The energy difference between the two approaches is even smaller than in the Zr case, e.g., 0.1 eV (~2 kcal/mol) at $L$ = 4.25 Å. The regiospecificity

(19) Lauher, J. W.; Hoffmann, R. *J. Am. Chem. Soc.* **1976**, *98*, 1729–1742.

(20) Electronic structures of $Cp_2U(CH_3)_2$ and $Cp_2UCl_2$ have been examined by the $X_\alpha$-SW method: Bursten, B. E.; Fang, A. *J. Am. Chem. Soc.* **1983**, *105*, 6495–6496.

(21) (a) $Cp^*_2ZrH_2$ reacts with CO at low temperature. The observable adduct appears to contain CO in the central position but may well be the thermodynamic product: Marsella, J. A.; Curtis, C. J.; Bercaw, J. E.; Caulton, K. G. *J. Am. Chem. Soc.* **1980**, *102*, 7244–7246. (b) The insertion of $Ph_2CN_2$ into a Zr–$CH_3$ bond of $Cp_2Zr(CH_3)_2$ yields an adduct, the structure of which reflects the lateral attack of $Ph_2CN_2$: Gambarotta, S.; Basso-Bert, M.; Floriani, C.; Guastini, C. *J. Chem. Soc., Chem. Commun.* **1982**, 374–375.

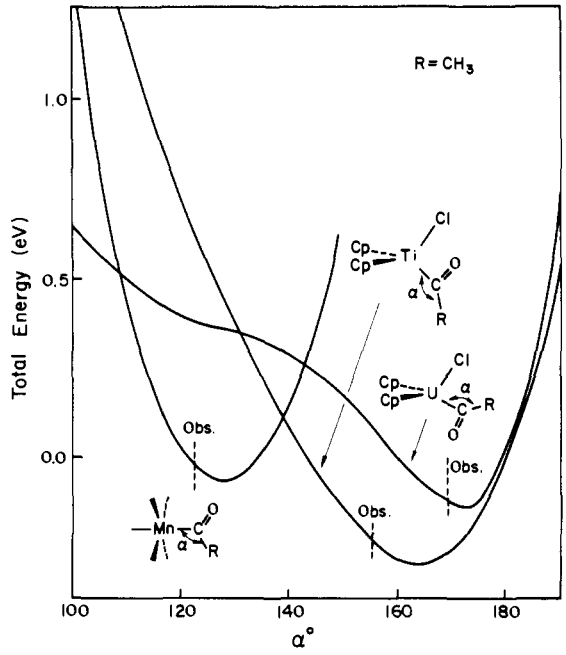


**Figure 2.** Potential energy curves of $Cp_2Ti(COCH_3)Cl$, $Cp_2U(COCH_3)Cl^{2+}$, and $Mn(CO)_5(COCH_3)$ as a function of M–C–C($CH_3$) angle $\alpha$. The experimentally observed angle $\alpha$ for $Cp_2Ti(COCH_3)Cl$, $Cp^*_2Th[COCH_2C(CH_3)_3]Cl$, or $[Mn(CO)_4(COCH_3)(COPh)]^-$ is located by a mark "Obs." in each corresponding curve.

for A, albeit weak, can be attributed again to the better overlap between the vacant orbital of type **7a** of $Cp_2U(CH_3)_2^{2+}$ and the CO lone pair **7b**. We have also computed the analogous potential energy curves for the U system with two more electrons, $Cp_2U(CH_3)_2$ + CO, in which the U atom now has a $5f^2$ $6d^0$ configuration. The energy profile obtained is very similar to the one in Figure 1, bottom. The presence of the two additional electrons in f orbitals does not affect the choice of preferred stereocourse for CO attack.

We should note here that the calculated small energy barriers are in harmony with what we know from experiment. That is, CO insertion into $d^0$ $Cp_2MR_2$ complexes is an extremely facile process. Although an activation energy for such a process has not been experimentally determined, CO insertion into $Cp_2Zr(CH_3)_2$ is known to occur at temperatures as low as −130 °C in solution. Carbonylation of the actinide complexes might well be still more facile. In toluene solution at −80 °C, $Cp_2^*Th(CH_3)_2$ and $Cp_2^*U(CH_3)_2$ take up 2 equiv of CO (<1 atm) within 1 h.[2e] Even a compound with a bulkier alkyl group, $Cp_2^*Th(CH_2{}^tBu)Cl$, reacts rapidly with 1 equiv of CO at room temperature,[7] and the reaction of $Cp_2^*M[CH_2Si(CH_3)_3]Cl$ (M = Th, U) takes place at −78 °C.[2a]

CO attack via the favorable route A should lead to an immediate acyl product of "O-outside" structure **1**. In contrast, the isolated acyl complexes of group 4 metals reveal only the alternative "O-inside" structure **2**. This apparent contradiction was resolved by Erker and Rosenfeldt,[9] who detected spectroscopically an intermediate of structure **1** in the carbonylation of $Cp_2Zr(p\text{-}CH_3C_6H_4)_2$, $Cp_2Zr(p\text{-}CH_3OC_6H_4)$, and $Cp_2Zr(CH_3)_2$. The unstable intermediate isomerizes to structure **2** irreversibly, by a mechanism which will be analyzed later.

### Acyl-Ligand Coordination

To investigate more closely the coordination modes of acyl ligands, we have calculated potential energy curves for acetyl pivoting in $Cp_2Ti(COCH_3)Cl$ and $Cp_2U(COCH_3)Cl^{2+}$. The model uranium complex could be a model for the known $Cp_2^*Th(COCH_2{}^tBu)Cl$. The first variable we vary is the M–C–$CH_3$ angle $\alpha$, while all other geometrical parameters are still kept fixed for each molecule. Figure 2 superimposes the three energy curves, including for comparison also the energy of an acyl ligand in $Mn(CO)_5(COCH_3)$ so rotated.[22] As Figure 2 shows, the optimum mode of acyl coordination in $Mn(CO)_5(COCH_3)$ is the $\eta^1$ type ($\alpha$ = 128°). On the other hand, the acyl ligands of $Cp_2Ti(COCH_3)Cl$ and $Cp_2U(COCH_3)Cl^{2+}$ tend to bend toward an $\eta^2$ geometry, pronouncedly so in the latter molecule. The calculated trend is in good agreement with the experimentally observed structures of $Cp_2Ti(COCH_3)Cl$ and $Cp_2^*Th(COCH_2{}^tBu)Cl$. Note that in calculating the curves in Figure 2 we assumed the orientation of the $\eta^2$ acyl (O-inside or O-outside) to be the same as observed for each. We will turn to the interesting choice between the two conformations of the acyl in a moment.

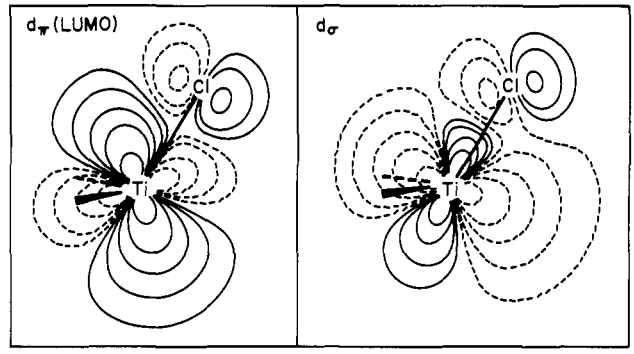


**Figure 3.** Contour plots of the two frontier orbitals, $d_\pi$ and $d_\sigma$ of a $Cp_2TiCl^+$ fragment. The orbitals are shown in the *xy* plane. The contour levels of each diagram are ±0.01, ±0.02, ±0.055, ±0.1, ±0.2, and ±0.4. The solid lines trace contours of one sign of $\psi$, the dashed lines of the opposite sign.

The diversity of optimal angles $\alpha$ in Figure 2 may be easily understood in terms of optimal interaction between frontier orbitals of each metal fragment and acetyl. Knowing that a bent $d^0$ $Cp_2M$

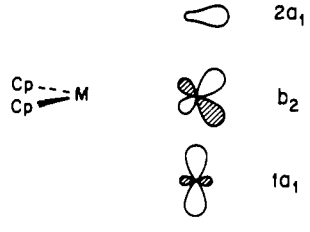


**8**

unit has three low-lying vacant orbitals, $1a_1$, $b_2$, and $2a_1$ (**8**),[20] one may derive the frontier orbitals of a $d^0$ $Cp_2MX^+$ fragment. The addition of a ligand X (X = $R^-$, $Cl^-$, etc.) destabilizes one combination and rehybridizes the two acceptor orbitals remaining at low energy.[23] One is a somewhat perturbed version of the $1a_1$ which is the LUMO of $d^0$ $Cp_2MX^+$. Toward a fourth ligand L, an acyl group in this case, this LUMO exhibits $\pi$ symmetry with respect to the M–L bond. For simplicity let us abbreviate this MO as $d_\pi$. The other acceptor orbital is locally of $\sigma$ type, thus named $d_\sigma$ here. The two low-lying vacant orbitals are plotted for $Cp_2TiCl^+$ in Figure 3.

An acyl ligand, $CH_3CO^-$, brings two donor orbitals. The high-lying HOMO, $n_-$, consists mostly of a carbon lone pair with an out-of-phase admixture of the oxygen p orbital. The lower donor orbital, $n_+$, is an in-phase combination of the same orbitals, with a larger oxygen p component. The $n_-$ and $n_+$ orbitals, which are sketched in **9**, find a symmetry match with the $Cp_2TiCl^+$ $d_\pi$ and $d_\sigma$ orbitals, respectively. The dominant interaction occurs between $n_-$ and $d_\pi$; this is, in fact, the major factor governing the $\eta^2$ coordination mode of acyl in $Cp_2Ti(COCH_3)Cl$ and also in $Cp_2Zr(COCH_3)(CH_3)$.

(22) Studies of the carbonylation of $RMn(CO)_5$ to give $RCOMn(CO)_5$ are numerous. For example, Closson, R. D.; Kozikowski, J.; Coffield, T. H. *J. Org. Chem.* **1957**, *22*, 598. Noack, K.; Calderazzo, F. *J. Organomet. Chem.* **1967**, *10*, 101–104. The $\eta^1$-acyl structure was observed by X-ray analysis for a related molecule: *cis*-$(CO)_4Mn(COCH_3)(COC_6H_5)$. See: Casey, C. P.; Bunnell, C. A.; Calabrese, J. C. *J. Am. Chem. Soc.* **1976**, *98*, 1166–1171.

(23) (a) Hofmann, P.; Stauffert, P.; Schore, N. E. *Chem. Ber.* **1982**, *115*, 2153–2174. (b) Silver, M. E.; Eisenstein, O.; Fay, R. C. *Inorg. Chem.* **1983**, *22*, 759–770.

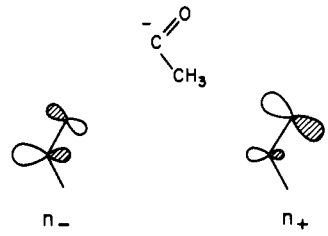


9

The in-phase combination of the n_ and $d_\pi$ orbitals yields the HOMO of $Cp_2Ti(COCH_3)Cl$. The primary bonding is set by an overlap between the large lobe of $d_\pi$ and the carbon lone-pair portion of n_, as shown in **10**. This represents the metal-to-carbon

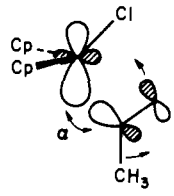


10

$\sigma$ bonding for the O-inside conformer. There is a further interaction available between the O p in n_ and the smaller lobe of $d_\pi$. This additional interaction will be increased as acyl pivots toward an $\eta^2$ structure, thus stabilizing the HOMO.

Figure 4 shows how the frontier orbitals evolve as a function of $\alpha$. The HOMO level (2a′) first goes down in energy as the acyl ligand bends from an $\eta^1$ geometry, falling to a minimum at $\alpha \approx 157°$. This energy profile can be anticipated from the phase relationship of **10**. The total energy curve for the acyl pivoting of $Cp_2Ti(COCH_3)Cl$ in Figure 2, having a minimum at $\alpha \approx 165°$, follows well the HOMO energy change. The empty 3a′ orbital, which is the antibonding counterpart of **10**, moves up steeply on going from $\eta^1$ to $\eta^2$. In the course of its ascent 3a′ crosses another empty orbital 2a″. The 2a″ stays low in energy over a wide range of bending angle $\alpha$, and plays a critical role as the low-lying LUMO of the $\eta^2$-acyl complexes governing their unique reactivity. It consists mostly of the acyl $\pi^*$ orbital lying perpendicular to the $xy$ plane, thus designated $\pi^*_{CO}$, stabilized through an interaction with an empty d orbital of $Cp_2TiCl^+$. Our interpretation of the $\eta^2$-acyl coordination in $Cp_2Ti(COCH_3)Cl$, based on the character of its HOMO, parallels that of the isostructural $\eta^2$-acyl complex, $Cp_2Zr(COCH_3)(CH_3)$.

For the actinide molecule $Cp_2U(COCH_3)Cl^{2+}$, we observed a similar stabilization of the HOMO as the acyl bends. Note that the acyl orientation is now O-outside. As shown in the Walsh diagram of Figure 5, the HOMO has a minimum at $\alpha \approx 173°$; this is the primary reason the acyl ligand tends to bend toward an $\eta^2$ geometry (see the total energy curve in Figure 2). Again the HOMO comprises mostly the acyl n_ orbital with U d orbitals as well as f orbitals mixing in. As a consequence of the additional f orbital contribution, the detailed shape of the HOMO is somewhat complicated and its contour map is drawn in **11**, where

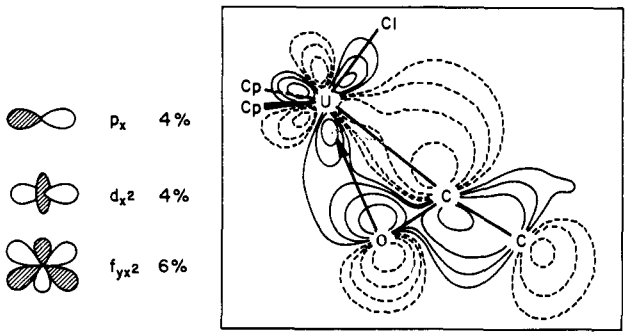


11

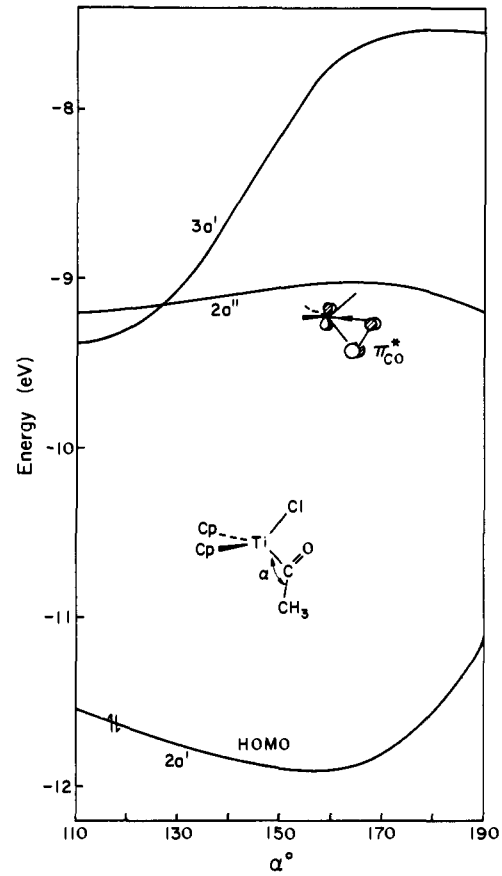


**Figure 4.** Walsh diagram for acyl pivoting ($\alpha$) in $Cp_2Ti(COCH_3)Cl$. The orientation of acyl is O-inside.

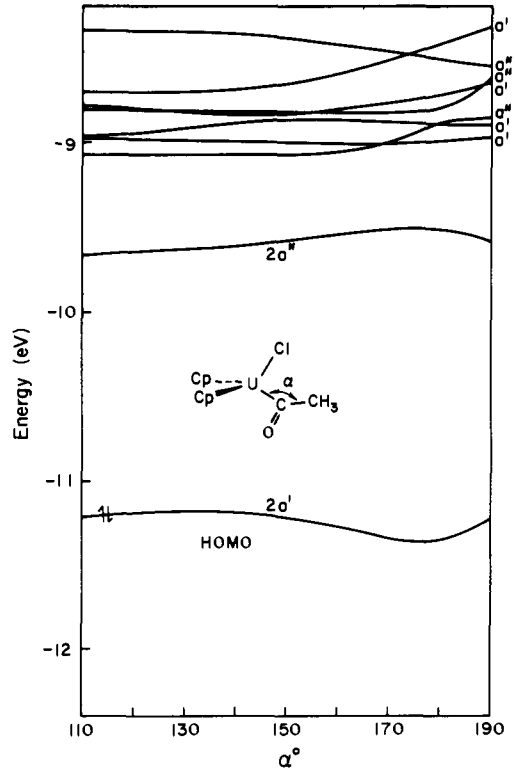


**Figure 5.** Walsh diagram for acyl pivoting ($\alpha$) in $Cp_2U(COCH_3)Cl^{2+}$ with a $5f^0$ electronic configuration. The acyl orients as O-outside.

the composition of the U orbitals in the HOMO is also shown. From the contour map of **11**, it is clear how the $\eta^2$-acyl structure stabilizes the HOMO. The carbon and oxygen orbital lobes in the acyl n_ orbital overlap nicely with this U hybrid orbital. To

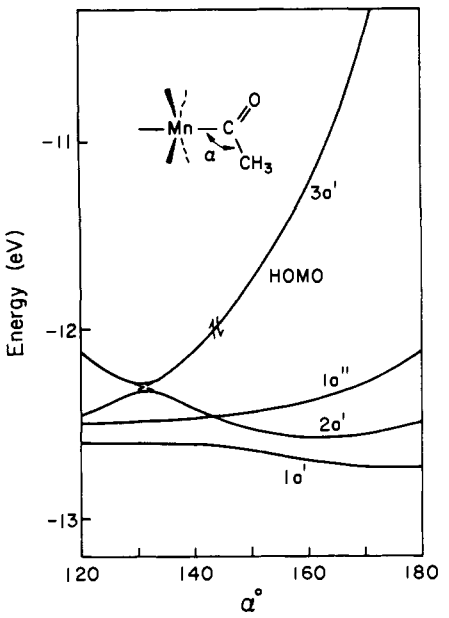


**Figure 6.** Walsh diagram for acyl pivoting ($\alpha$) in $Mn(CO)_5(COCH_3)$. The LUMO is at around −9 eV in energy and is not shown in the figure.

investigate how much U f orbitals participate in the net U–acyl bonding, we performed a population analysis for $Cp_2U(COCH_3)Cl^{2+}$ at $\alpha = 170°$. The calculated overlap populations associated with U f orbitals are 0.062 (U(f)–C) and 0.046 (U(f)–O), while the total U–C and U–O overlap populations are 0.372 and 0.0723, respectively.

The LUMO in the Walsh diagram is very much similar to the 2a″ of $Cp_2Ti(COCH_3)Cl$ in Figure 4. It contains the acyl $\pi^*_{CO}$ orbital with a strong admixture of U f orbitals. Higher in energy there are seven U f orbitals. There is an interesting question as to where the electrons go into the system in the $f^2$ complexes, e.g., $Cp_2^*U(COR)Cl$. If they reside in the 2a″, then the CO bond should be much weakened. The observed CO stretching frequencies are 1546 and 1559 $cm^{-1}$ in $Cp_2^*Th[CO(N(CH_3)_2)]Cl$ and the analogous U derivative, respectively.[8a] The trend is opposite to expectations based on 2a″ occupation. It may be that the CO vibration is strongly coupled with M–C and M–O modes, for these acyls are far from normal, or, alternatively, our 5f parameters put the mainly f orbitals too high, and really they should be below the 2a″.

The Walsh diagram for the acyl pivoting in $Mn(CO)_5(COCH_3)$ is shown in Figure 6. In contrast to the group 4 metal and the actinide systems, the HOMO of $Mn(CO)_5(COCH_3)$ moves to higher energy as the acyl ligand bends from the $\eta^1$ minimum at $\alpha \approx 131°$. The reason behind this trend is rather straightforward. The $Mn(CO)_5^+$ fragment, having a $d^6$ electronic configuration, carries an acceptor orbital of $a_1$ symmetry, **12**,[24] while two $d_\pi$

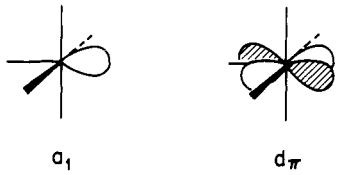


**12** **13**

orbitals are filled. The $d_\pi$ orbitals are mutually orthogonal, and one of them is depicted in **13**. The interaction of the occupied $d_\pi$ **13** with the occupied $n_-$ of acyl turns out to be repulsive in the HOMO of $Mn(CO)_5(COCH_3)$, when the acyl ligand coordinates to Mn in an $\eta^2$ mode. This reasoning carries over to an analysis of the geometrical preference of many other $\eta^1$-acyl complexes, e.g., $Fe(HBpz_3)(CO)_2(COCH_3)$,[25] $Ni(PMe_3)_2Cl(COR)$,[26] and $Rh(OEP)(COH)$.[27]

An interesting conclusion follows from Figure 6. For an acyl complex with two electrons less than $Mn(CO)_5(COR)$, $\eta^2$-acyl bonding should become feasible. The HOMO (3a′) in Figure 6 is empty for the $d^4$ electron system. Then the lower 2a′ orbital, consisting of the in-phase combination of a metal $d_\pi$ and the acyl $n_-$, governs the geometry of the coordinated acyl ligand. The 2a′ molecular orbital is analogous to the HOMO (2a′) of $Cp_2Ti(COCH_3)Cl$ in Figure 4, which makes the $\eta^2$-acyl structure possible.

Indeed acyl compounds of this type, $V(\eta^2\text{-}COC_3Ph_3H_2)(CO)_3(Ph_2AsCH_2CH_2PPh_2)$,[28a] $V(\eta^2\text{-}COPh)(CO)_3(dppe)$ (**14a**),[28b] and $Mo(\eta^2\text{-}COCH_2SiMe_3)Cl(CO)(PMe_3)_3$ (**14b**),[28c] have been synthesized. Interestingly, in $Mo(COCH_3)(S_2CNMe_2)(CO)(PMe_3)_2$ (**14c**) the acyl ligand does not pivot toward an $\eta^2$ form,

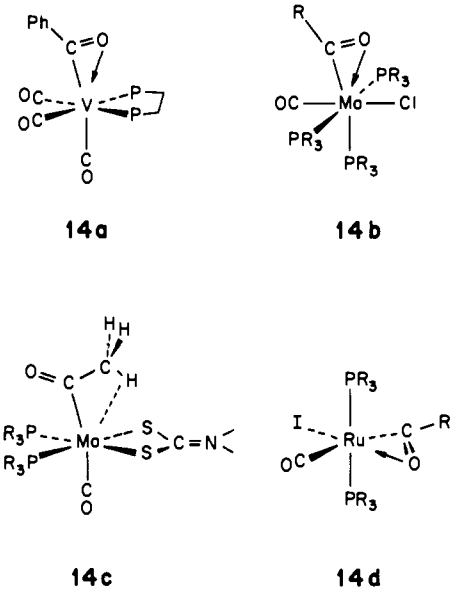


**14a** **14b**

**14c** **14d**

but moves in the opposite direction by virtue of a strong interaction with a $\beta$-C–H bond of acyl.[28c] Not unrelated to the $\eta^2$-acyl complexes of the $d^4$ $M(COR)L_5$ is $d^6$ $Ru(\eta^2\text{-}COR)I(CO)(PPh_3)_2$ (**14d**),[28d] where a $d_\pi$ orbital in the equatorial plane of the $RuI(CO)(PPh_3)_2^+$ fragment is vacant and behaves like the $d_\pi$ of $Cp_2TiCl^+$ in Figure 3. The electronic structures and bonding of the vanadium complexes will be discussed elsewhere.[29]

### O-Inside vs. O-Outside Conformations

Let us now turn to the interesting geometrical choice between the O-outside **1** and O-inside **2** isomers. In an attempt to compare energies of the two conformers of $Cp_2Ti(COCH_3)Cl$, we have calculated potential energy surfaces varying the Ti–C–C angle $\alpha$ and the Cl–Ti–C angle $\beta$ independently, as shown in **15a** and **15b**. The parameter $\alpha$ is the one used for plotting the energy curve of Figure 2. The geometry of the $Cp_2TiCl$ portion was common and kept fixed for both isomers. The calculated surfaces

(24) The orbitals of $M(CO)_5$ fragments have been extensively described. See, for instance: (a) Elian, M.; Hoffmann, R. *Inorg. Chem.* **1975**, *14*, 1058–1076. (b) Hoffmann, R. *Science* **1981**, *211*, 995–1002. (c) Hoffmann, R. *Angew. Chem., Int. Ed. Engl.* **1982**, *21*, 711–724.

(25) Cotton, F. A.; Frenz, B. A.; Shaver, A. *Inorg. Chim. Acta* **1973**, *7*, 161–169.

(26) (a) Huttner, O.; Orama, O.; Bejenke, V. *Chem. Ber.* **1976**, *109*, 2533–2536. (b) Carmona, E.; Gonzalez, F.; Poveda, M. L.; Atwood, J. L.; Rogers, R. D. *J. Chem. Soc., Dalton Trans.* **1980**, 2108–2116.

(27) Wayland, B. B.; Woods, B. A.; Pierce, R. *J. Am. Chem. Soc.* **1982**, *104*, 302–303.

(28) (a) Franke, U.; Weiss, E. *J. Organomet. Chem.* **1979**, *165*, 329–340. (b) Schiemann, J.; Weiss, E. *Ibid.* **1983**, *255*, 179–191. (c) Carmona, E.; Sanchez, L.; Marin, J. M.; Poveda, M. L.; Atwood, J. L.; Priester, R. D.; Rogers, R. D. *J. Am. Chem. Soc.* **1984**, *106*, 3214–3222. (d) Roper, W. R.; Taylor, G. E.; Waters, J. M.; Wright, L. J. *J. Organomet. Chem.* **1979**, *182*, C46–C48.

(29) Schiemann, J.; Weiss, E.; Hofmann, P., in preparation.

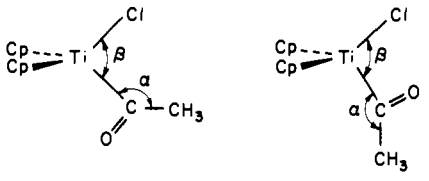

15a 15b

are presented in Figure 7a and Figure 7b for the O-outside and O-inside conformations, respectively. The potential surface of Figure 7b has a minimum at $\alpha = 165°$ and $\beta = 112°$, corresponding to the O-inside $\eta^2$ structure **2**. This minimum is 0.39 eV (9 kcal) more stable than that of the O-outside $\eta^2$ structure **3** in Figure 7a, which appears at $\alpha = 165°$ and $\beta = 85°$. The result agrees well with the experimental finding that only O-inside structures were found by the X-ray structure analyses for $Cp_2Ti(COCH_3)Cl$ and for its Zr congener, $CpZr(COCH_3)(CH_3)$.

However, the most interesting feature of the energy surface of Figure 7a is the presence of two potential minima for the O-outside conformation. One is for the aforementioned $\eta^2$ type **1**, and the other corresponds to an $\eta^1$-acyl coordination, appearing at $\alpha = 100°$ and $\beta = 120°$. This finding will be important when we consider the full reaction pathway of $Cp_2Zr(CH_3)_2 + CO$ later.

Before examining the electronic reasons for this unexpected existence of an $\eta^1$ minimum, we take a look at the origin of the different stability of the two $\eta^2$ structures, **1** and **2**. The orientational preference is again a consequence of the better overlap between the occupied acyl $n_-$ (**9**) and the vacant $d_\pi$ (Figure 3) of the $d^0$ $Cp_2TiCl^+$ fragment. For the O-inside orientation, the larger lobe of $d_\pi$ can overlap with the larger lobe on carbon of $n_-$. The smaller lobes of both frontier orbitals also retain a good overlap with each other. On the other hand, the O-outside orientation has a smaller $d_\pi$–$n_-$ interaction, because the larger $d_\pi$ lobe now faces the smaller lobe on oxygen of $n_-$ and vice versa. This situation is drawn schematically in **16a** and **16b**, where the

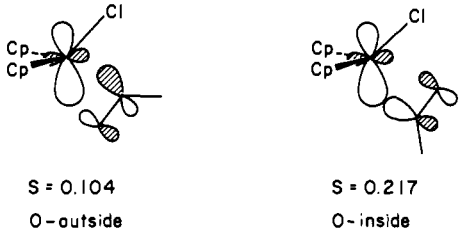


16a 16b

calculated overlaps, $S$, between the $d_\pi$ and $n_-$ orbitals for the two acyl orientations are also compared. The different magnitudes of the overlap integrals lead to a different stability of the HOMO of $Cp_2Ti(COCH_3)Cl$ as shown in the interaction diagrams for both orientations in Figure 8. The HOMO of the O-inside isomer is more stabilized, owing to the better $d_\pi$–$n_-$ interaction, which in turn gives a lower total energy.

Next we consider an actinide complex, $Cp_2U(COCH_3)Cl^{2+}$. Figure 9 shows the computed potential energy surfaces as a function of the U–C–C angle $\alpha$ and the C–U–Cl angle $\beta$ for the two acyl conformations. The two surfaces are similar in shape to those for $Cp_2Ti(COCH_3)Cl$ in Figure 7. However, the O-outside minimum at $\alpha = 170°$ and $\beta = 96°$ is now lower in energy than the O-inside minimum at $\alpha = 170°$ and $\beta = 112°$. The energy difference is merely 0.03 eV, 0.7 kcal/mol, and the stabilities of the two minima are essentially equal. Experimentally $Cp_2^*Th(COCH_2{}^tBu)Cl$ is known to assume the O-outside configuration, while for the related carbamoyl complexes, $Cp^*_2M(CONR_2)Cl$ (M = Th, U), the two conformations coexist either in solution or in crystal. $Cp^*_2Th(COC_6H_5)Cl$ has an O-inside structure.[8b] The computed potential surface for the O-outside conformation contains an additional minimum at $\alpha = 105°$ and $\beta = 120°$, though this minimum is a shallow one. It corresponds to an $\eta^1$ acyl structure, just as in the Ti case.

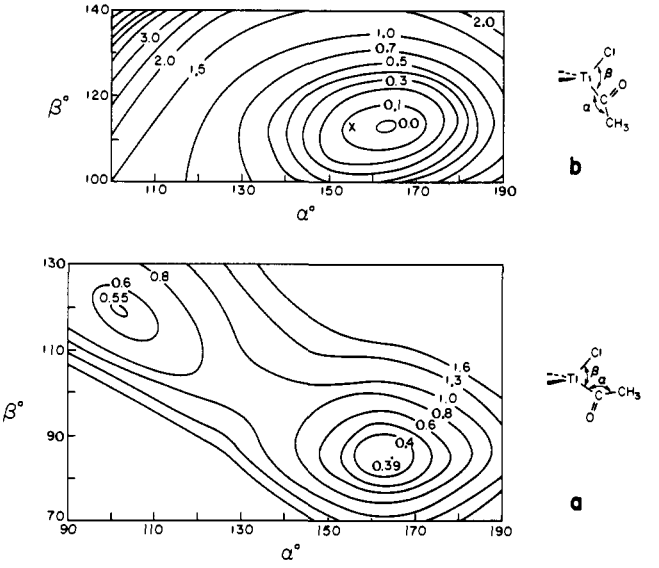


**Figure 7.** Potential energy surfaces as a function of $\alpha$ and $\beta$ for the O-inside (top) and O-outside (bottom) orientations of acyl in $Cp_2Ti(COCH_3)Cl$. The point marked by X in b indicates the experimentally observed structure of $Cp_2Ti(COCH_3)Cl$.

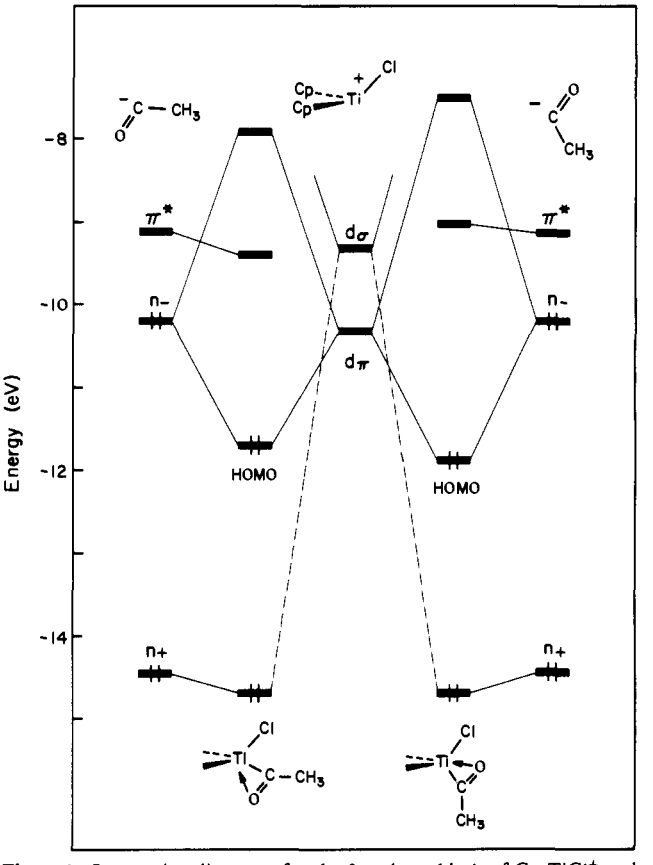


**Figure 8.** Interaction diagrams for the frontier orbitals of $Cp_2TiCl^+$ and $COCH_3^-$ in the $\eta^2$ O-outside (left) and $\eta^2$ O-inside (right) structures of $Cp_2Ti(COCH_3)Cl$.

The $Cp_2UCl^{3+}$ fragment carries a vacant $d_\pi$ orbital, **17**, like the one plotted for $Cp_2TiCl^+$ in Figure 3. Although the shape of **17** is essentially analogous to the $Cp_2TiCl^+$ $d_\pi$ orbital, its two lobes pointing toward the vacant site are nearly the same in size. Thus the two acyl orientations should not differ in their $d_\pi$–$n_-$ interactions as much as they do in the Ti complex. This is probably one reason why O-outside and O-inside conformers of $Cp_2U(COCH_3)Cl^{2+}$ are energetically well balanced. There appears to be another factor coming in. The U atom has vacant f orbitals

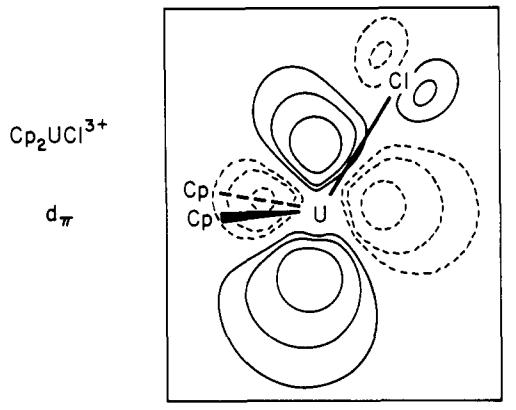


17

(in addition to $d_\pi$) which can interact with the occupied acyl $n_-$ orbital. The outcome is a complicated hybridization of d and f orbitals in the HOMO of $Cp_2U(COCH_3)Cl^{2+}$, the contour map of which has been shown in **11** for the O-outside orientation. The f orbitals mix into the HOMO in such a way that the hybrid-$n_-$ overlap becomes nearly equal for the two conformers. One may see in **11** that reversing the acyl orientation from O-outside to O-inside will not weaken the interaction between U and acyl.

We now come back to the unexpected double minimum found in the potential energy surfaces of the O-outside conformers in Figures 7a and 9a. Our eventual aim in this portion of the study is to gain insight into Erker's experiment on the CO insertion process of $Cp_2ZrR_2$, so that we shift our theoretical analysis from the Ti system to $Cp_2Zr(COCH_3)CH_3$ at this point. As will be shown soon, our conclusions based on the calculations for $Cp_2Ti(COCH_3)Cl$ carry over well to the Zr case.

To check if the energetics obtained for $Cp_2Ti(COCH_3)Cl$ are not particular to the Ti system, we computed also the potential surfaces for O-outside and O-inside isomers of $Cp_2Zr(COCH_3)(CH_3)$. The geometrical optimization was upgraded by allowing both $CH_3$ and $COCH_3$ ligands to move, thus varying independently three parameters, $\alpha$, $\beta'$, and $\gamma$, as defined in **18**.

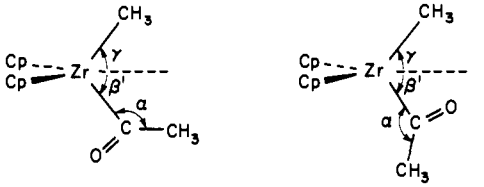


18a




18b

The sum of the new variables, $\beta'$ and $\gamma$, corresponds to $\beta$ in **15a** and **15b**. Again one $\eta^2$ minimum was found for **18b** at $\alpha = 170°$, $\beta' = 55°$, and $\gamma = 60°$, while for **18a** two minima showed up at $\alpha = 110°$, $\beta' = 55°$, and $\gamma = 50°$, and at $\alpha = 170°$, $\beta' = 25°$, and $\gamma = 60°$, being the $\eta^1$ and $\eta^2$ structures, respectively. The $\eta^2$ O-inside geometry is most stable of all. The $\eta^2$ O-outside is about 5 kcal/mol higher in energy than that, and the $\eta^1$ O-outside is still less stable by 5 kcal/mol.

The presence of two minima for the O-outside conformation means that there is an energy barrier on going from $\eta^1$ to $\eta^2$, and vice versa. The $\eta^1$ geometry carries 16 electrons at the metal center. Then the attachment of the oxygen lone pair to the electron-deficient metal center, in the $\eta^2$ coordination mode, makes the molecule an 18-electron compound. It is rather surprising that, depending on the acyl orientation, the acyl pivoting, an interconversion between 16- and 18-electron systems, should pass through a barrier. Let us try to understand the reason behind this. In the $\eta^1$ structures, the phase relationship for the important $d_\pi$–$n_-$ interaction is set so as to form an overlap between the large lobe of $d_\pi$ and the carbon lobe of acyl $n_-$. The HOMO of each

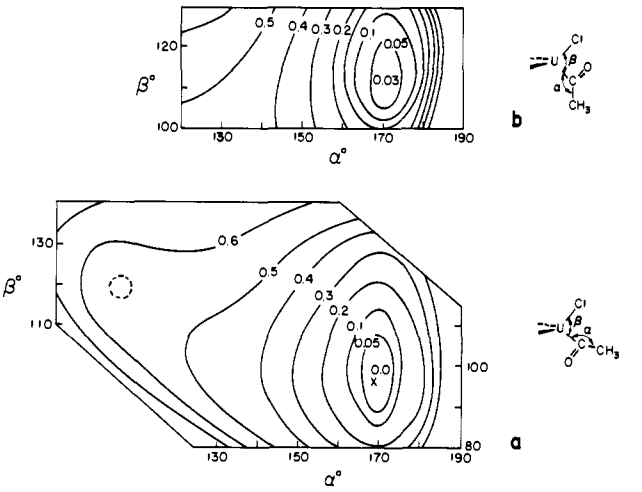


**Figure 9.** Potential energy surfaces as a function of $\alpha$ and $\beta$ for the O-inside (top) and O-outside (bottom) orientation of acyl in $Cp_2U(COCH_3)Cl^{2+}$. The point marked × is the experimentally observed structure of $Cp^*_2Th[COCH_2C(CH_3)_3]Cl$.

$\eta_1$ complex, O-outside or O-inside, is made up of this bonding combination of $d_\pi$ and $n_-$; see **19a** and **20a**.

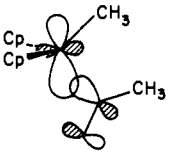


$\eta^1$ O-outside

19a

barrier

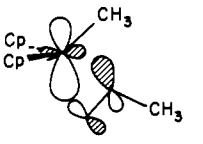


$\eta^2$ O-outside

19b

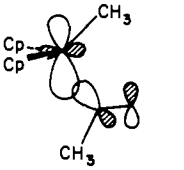


$\eta^1$ O-inside

20a

no barrier

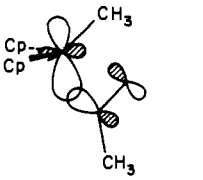


$\eta^2$ O-inside

20b

The notable difference between **19a** and **20a** lies in their nodal properties. It is clear from **20a** and **20b** that the $\eta^1$ O-inside structure relaxes to the $\eta^2$ structure without destroying the phase-match between $d_\pi$ and $n_-$. The $\eta^1 \rightarrow \eta^2$ transformation occurs smoothly, simply increasing the interaction between the small lobe of $d_\pi$ and the oxygen lobe of $n_-$. Therefore, the O-inside conformer ends up with a single minimum of the $\eta^2$ type. On the contrary, the $\eta^1 \rightleftarrows \eta^2$ interconversion for the O-outside case involves a phase discontinuity. The carbon lobe has to switch its phase during the acyl pivoting, and the same for the oxygen lobe. at the place where the phase discontinuity takes place, the molecule loses its $d_\pi$–$n_-$ bonding interaction, thus causing an energy barrier.

The origin of the barrier described above is evident in the Walsh diagram of Figure 10 for the O-outside $\eta^1 \rightleftarrows \eta^2$ process. The HOMO on each side, which is **19a** or **19b**, tends to correlate to the LUMO on the other side. Each HOMO ascends in energy until they meet each other at a maximum inbetween the $\eta^1$ and $\eta^2$ energy wells. What actually happens is that there is a strongly avoided crossing between the LUMO and the HOMO, because of the low $C_s$ molecular symmetry. The HOMO energy profile is responsible for the double minimum found in the potential energy surfaces for the $Cp_2M(COCH_3)X$ complexes.

Noteworthy here is the metal–oxygen antibonding interaction seen in **19a**. A consequence is the large M–C–O angle of ~ 130–135° at the $\eta^1$ O-outside minima found by our calculations

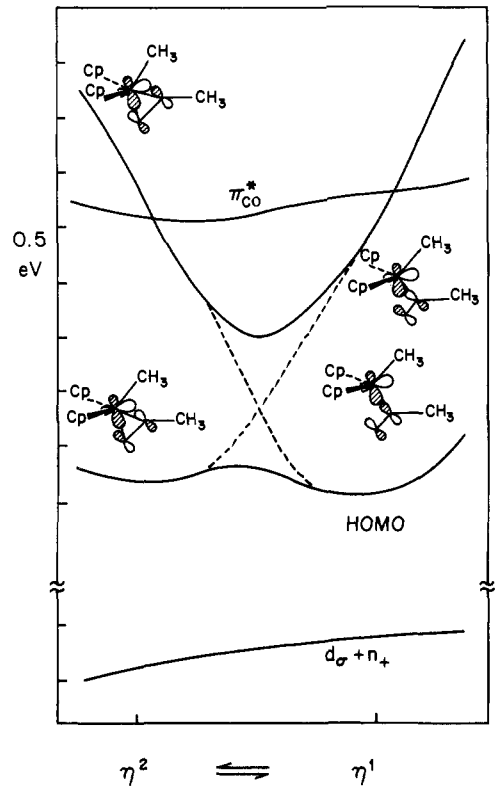


**Figure 10.** Orbital correlation diagram for the interconversion between $\eta^1$ and $\eta^2$ structures of the O-outside acyl orientation in $Cp_2Zr(COCH_3)(CH_3)$.

on the Ti and Zr complexes. Incidentally, a related Zr complex, $Cp_2Zr(CH_2PPh_2)Cl$, has been recently synthesized.[30] Its X-ray diffraction study shows that the $CH_2PPh_2$ ligand is bound to Zr in an $\eta^1$ manner, as indicated in **21**. This complex is analogous

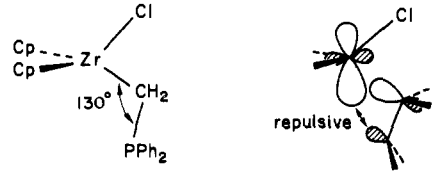


**21** **22**

to the $\eta^1$ O-outside structure **19a** of $Cp_2Zr(COCH_3)CH_3$. The $CH_2PPh_2^-$ ligand has a HOMO made out of an out-of-phase combination of carbon and phosphorus lone-pair orbitals, which is very similar to the $n_-$ orbital of $COCH_3^-$. Because of the antibonding interaction between the $d_\pi$ lobe and the phosphorus lone pair in **22**, the P atom tends to stay away from the electron-deficient Zr center with its 16-electron count, a result which would seem puzzling if it were not for these orbital symmetry arguments. The opening up of the Zr–C–P angle from its ideal tetrahedral angle of 109° is a result. The observed Zr–C–P angle is as large as 130°.[30] For details of the theoretical analysis of $Cp_2Zr(CH_2PPh_2)Cl$, the reader should refer to ref 23a where alternative geometries and steric effects for **21** have been discussed in detail. A double-minimum situation similar to the one described above has also been found for $Cp_2Zr(S_2CH)Cl$ by Silver, Eisenstein, and Fay.[23b]

### The $\eta^2$ O-Outside to $\eta^2$ O-Inside Rearrangement

As discussed in an earlier section of this paper, we believe a CO molecule attacks the central metal at a lateral site of $Cp_2MRX$ or $Cp_2MR_2$. For M = Zr, the isolable product assumes the $\eta^2$ O-inside structure, **2**, so that the formation of an immediate kinetic product $\eta^2$ O-outside, **1**, should be followed by an isomerization

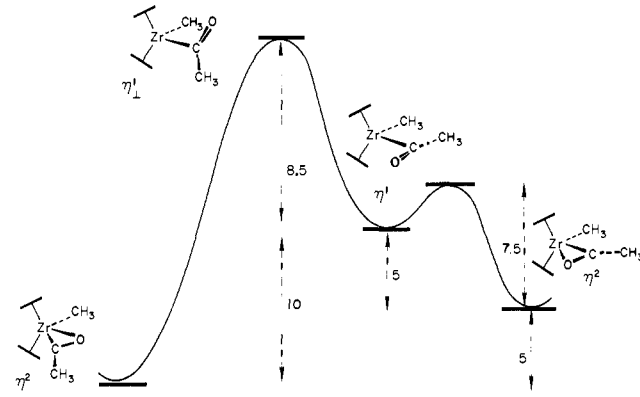


**Figure 11.** Computed energy profile for $Cp_2Zr(COCH_3)(CH_3)$ along the proposed isomerization pathway from the $\eta^2$ O-outside structure, which is the kinetic product of CO insertion into $Cp_2Zr(CH_3)_2$, to the thermodynamically more stable form, $\eta^2$ O-inside. Energies are shown in kcal/mol units.

**Scheme I**

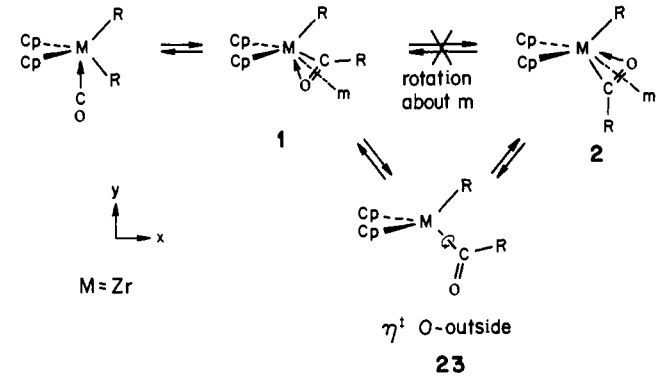


step leading to the thermodynamically more stable structure **2**. We want to understand here how the isomerization takes place.

The simplest isomerization process, i.e., the direct rotation of the $\eta^2$ acyl about the axis *m* in Scheme I, is not likely to occur. A bent $Cp_2M$ fragment is known to form strong bonds with ligands only when the coordination occurs in the *xy* plane.[19] It is clear why this is so: the three frontier orbitals of $Cp_2M$, **8**, all lie in the plane. Thus the rotation of acyl about *m* would result in disruption of much of the bonding interaction between acyl and $Cp_2MR$, importantly the $n_-$–$d_\pi$ interaction. As a result, the calculated barrier to that rotation is fairly large, as large as 2.5 eV (58 kcal/mol) for $Cp_2Ti(COCH_3)Cl$ and only slightly smaller than that in the case of $Cp_2Zr(COCH_3)(CH_3)$.

We now propose an alternative route via the $\eta^1$ O-outside intermediate, **23**, which was unexpectedly found in our potential energy surfaces for acyl O-outside conformations of $Cp_2Ti(COCH_3)Cl$ and of $Cp_2Zr(COCH_3)(CH_3)$. The potential energy surfaces reveal that the transformation of **1** to **23** is an easier process than the direct rotation, requiring 7.5 kcal/mol for $Cp_2Zr(COCH_3)(CH_3)$,[31] and about 14 kcal/mol for $Cp_2Ti(COCH_3)Cl$.

The subsequent step from **23** to **2** consists of a rotation around the M–C single bond, passing through the "perpendicular" $\eta^1$ structure, **24**, as a transition state. To obtain a theoretical estimate of the rotation barrier, we optimized the transition state **24** for $Cp_2Zr(COCH_3)(CH_3)$, by varying the angles $\beta'$ and $\gamma$ as we did in **18b**, as well as the Zr–C–$CH_3$ angle $\alpha$ and the Zr–C–O angle $\alpha'$. The computed barrier is 8.5 kcal/mol, much smaller than the rotation about the axis *m*, as one might easily anticipate from the fact that the former is a rotation about the Zr–C single bond. At the transition state, **24**, the Zr–C–$CH_3$ angle $\alpha$ opens up slightly to 130°, in order to avoid a contact between the Cp ring and the

(30) Schore, N. E.; Hope, H. *J. Am. Chem. Soc.* **1980**, *102*, 4251–4253.

(31) In the calculations on the $Cp_2Zr(COCH_3)(CH_3)$ system, the position of the metal-bound methyl group was also optimized independently.

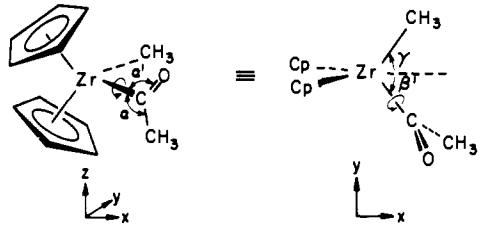

24

methyl group of acyl. The other optimized numbers include 120° for $\alpha'$ and 95° for $\gamma + \beta'$. The overall energy profile is now in our hands for the **1** → **2** isomerization of $Cp_2Zr(COCH_3)(CH_3)$. Figure 11 summarizes it in kcal/mol units. The net activation energy on going from the elusive $\eta^2$ O-outside structure to the thermodynamically stable $\eta^2$ O-inside form amounts to 13.5 kcal/mol. The experimentally observed activation free energy for the isomerization of $Cp_2Zr(COR)(R)$ ranges from 11.4 kcal/mol (R = $CH_3$) to 15.6 kcal/mol (R = *p*-tolyl or *p*-anisyl).[9] The agreement between the theoretical estimates and the experimental observations is surprisingly good, considering the approximate nature of our calculations.

For $Cp_2Ti(COCH_3)Cl$, there appeared to be steric problems at the transition state analogous to **24**. A rigid rotation of $COCH_3$ from $\eta^1$ O-outside meets a prohibitively high barrier of ~2.5 eV, due to the steric congestion associated with the smaller ionic radius of Ti compared with Zr. A better geometrical optimization could result in a reduction of the barrier,[32] but we think that the calculated large barrier provides us with an interesting hypothesis. If an acyl complex of the type $Cp_2M(COR)X$ (M = group 4 metals) is not allowed to undergo the rotation for steric reasons, then the CO insertion product of $Cp_2MRX$ may be unable to reach the stable O-inside $\eta^2$-acyl product. Two possibilities ensue. The metastable $\eta^2$ O-outside complexes of group 4 metals could be isolated. Alternatively, if the steps are reversible, the CO insertion process itself might not be seen, and other reaction channels followed. As a matter of fact, we know of no experimental evidence that acyl complexes of Ti, $Cp_2Ti(acyl)X$, are formed by CO insertion of $Cp_2TiRX$. Remember that $Cp_2Ti(COCH_3)Cl$ was synthesized from $Cp_2Ti(CO)_2$ by a reaction with $CH_3COCl$.[5]

The isolated product of $Cp_2^*Th[COCH_2{}^tBu]Cl$ possesses an $\eta^2$ O-outside geometry.[7] This fact and the potential energy surfaces in Figure 9 for the model complex, $Cp_2U(COCH_3)Cl^{2+}$, indicates that the kinetic $\eta^2$ O-outside product of CO insertion is thermodynamically stable too. The trimethylsilylmethyl derivatives, $Cp^*_2M[COCH_2Si(CH_3)_3]Cl$ (M = Th, U), which were formed by the reaction of $Cp^*_2M[CH_2Si(CH_3)_3]Cl$ with CO, were detected by $^1H$ NMR at low temperature.[33] Although their detailed structures are yet unknown, the molecules have been assigned bihaptoacyl structures. Not to be ruled out is the possibility that the two isomeric bihaptoacyl structures, $\eta^2$ O-outside and $\eta^2$ O-inside, of these actinide complexes are in equilibrium in solution. If the equilibrium exists, it is likely to occur via an $\eta^1$ O-outside intermediate, just as we think occurs for the zirconium congeners. Figure 9 shows that the $\eta^1$ O-outside minimum is 0.55 eV (12.6 kcal/mol) less stable than the $\eta^2$ O-outside structure. The activation energy for the $\eta^2 \rightarrow \eta^1$ transformation is about 0.55 eV as well, since the $\eta^1$ potential well is shallow. The barrier to the subsequent rotation leading to an $\eta^2$ O-inside structure would be sensitive to the bulk of acyl substituents and that of Cp*. Unfortunately, the synthesized actinide complexes are too large to treat by our calculations, but the potential surfaces of Figure 9 should aid us in considering the isomerization process. For the related carbamoyl complexes, $Cp^*_2M[CON(CH_3)_2]Cl$ (M = Th, U), the two $\eta^2$ conformations, **25a** and **25b**, are essentially equal

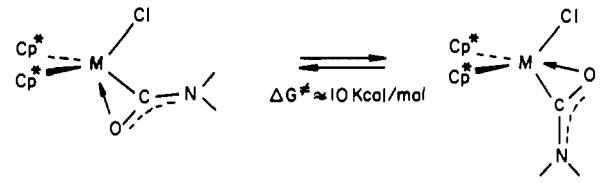


25a 25b

in free energy in solution. The observed activation free energy $\Delta G^\ddagger$ for their interconversion is ca. 10 kcal/mol.[8] The transformation from $\eta^2$ O-outside to $\eta^1$ O-outside of the carbamoyl complexes would require less energy than the one of the model $Cp_2U(COCH_3)Cl^{2+}$, because of the $\pi$ conjugation present between C–O and C–N bonds of the carbamoyl ligand.

### Reactivity of the $\eta^2$-Coordinated Acyls

We finally analyze the origin of the unique reactivity of acyl ligands in $Cp_2M(COR)X$. As mentioned in the Introduction, such $\eta^2$-acyl biscyclopentadienyl complexes exhibit a rich and promising chemistry. The dominant features of their reactivity have often been rationalized in terms of a contribution of the oxycarbene-type resonance hybrid **4b** to their ground-state properties, lending carbenoid character to the $\eta^2$-coordinated acyl ligands. In view of strong oxophilicity of group 4 metal and actinides,[34] one might anticipate that acyl ligands could adopt still another mode of coordination, as shown in **5**, where only an oxygen atom of the acyl is attached to the $d^0$ central metal, leaving a carbon site free.

In order to test whether, in fact, the alternative structure can be an intermediate in the many reactions associated with coordinated acyl ligands, we carried out a geometrical optimization for the two conformations, **26** and **27**, while the geometry of the acyl portion is unchanged, with a Zr–O distance of 2.15 Å. The electronic configuration of the carbene part is assumed to be singlet.[35] The structures **26** and **27** formally derive from carbon–metal bond disruption in the $\eta^2$ O-outside and $\eta^2$ O-inside structures, respectively. They are interrelated by a simple rotation

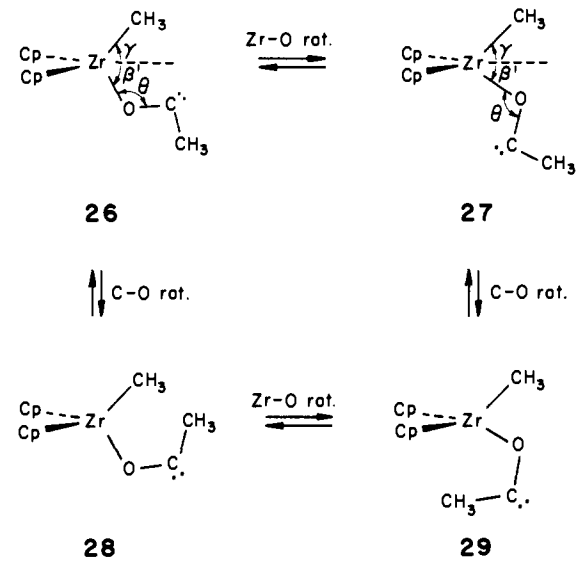


26 27

28 29

about the Zr–O bond, and rotation about the C–O bond from them gives two more isomers, **28** and **29**. From our geometrical search,

(32) In order to attenuate the steric problems at the transition state, we intentionally elongated the Ti–C(Cp) and Ti–C(acyl) distances from 2.388 to 2.5 Å, and from 2.07 to 2.197 Å, respectively. The longer distances are those used for calculations on $Cp_2Zr(COCH_3)CH_3$. The rotational barrier was decreased to 0.9 eV (21 kcal/mol), which is still higher in energy than the Zr case.

(33) See ref 2a, and ref 6 and 33 cited in that paper.

(34) (a) McDade, C.; Green, J. C.; Bercaw, J. E. *Organometallics* **1982**, *1*, 971–973. (b) Dias, A. R.; Salema, M. S.; Simoes, J. A. M. *Ibid.* **1982**, *1*, 971–973. (c) See ref 2, 3a, and Bruno, J. W.; Marks, T. J.; Morss, L. R. *J. Am. Chem. Soc.* **1983**, *105*, 6824–6832.

(35) The EH–HOMO/LUMO gap is about 1 eV for the zirconoxycarbene structures, as found for alkyl-alkoxycarbenes, which are singlet ground states. See, for instance: Davidson, E. R. "Singlet Triplet Energy Separations in Carbenes and Related Diradicals"; In "Diradicals"; Borden, W. T., Ed.; Wiley: New York, 1982; p 73.

we obtained the following results: (i) Each zirconoxy carbene structure, **26** or **27**, is a local minimum of the potential energy surface. (ii) The optimal Zr–O–C angles $\theta$ are both close to 180°, so that there is no practical difference in structure between **26** and **29**, and between **27** and **28**.[36] (iii) In our model calculations, the energies of **26** and **27** are both very high, ca. 2 eV higher than those of corresponding $\eta^2$ acyl geometries.

Although $Cp_2Zr(COCH_3)CH_3$ has local minima corresponding to zirconoxy carbene structures, it is a high-energy process for the molecule to move from its ground-state $\eta^2$-acyl structure to these metastable states. Therefore, the so-called carbene-type reactivity of such $\eta^2$-coordinated acyls is probably not derived from a preequilibrium with the oxycarbene isomers, **26**–**29**, which could subsequently undergo the observed reactions. Instead, the electronic properties of the ground-state $\eta^2$-acyl structures themselves should be responsible for the unique reactivity of acyl groups attached to $d^0$ $Cp_2MX$ fragments.

Recall here the molecular orbital diagrams of $Cp_2Ti(COCH_3)Cl$ in Figures 4 and 8, of $Cp_2U(COCH_3)Cl^{2+}$ in Figure 5, and of $Cp_2Zr(COCH_3)CH_3$ in Figure 10. A common feature of these diagrams is that they all possess a low-lying LUMO, **30**, made


$\pi^*_{CO}$ (LUMO) Carbene $\pi$ (LUMO)

**30** **31**

up of the acyl C–O $\pi^*_{CO}$ which is perpendicular to the acyl plane. The LUMO may appear even lower in energy than the $\pi^*_{CO}$ orbital of acyl itself, because metal *xz* and/or *yz* orbitals can mix in $\pi^*_{CO}$, thus pushing it *down*. The presence of a low-lying vacant $\pi^*_{CO}$ makes the acyl carbon strongly electrophilic, which accounts for the reactivity of these $d^0$ $\eta^2$-acyl compounds. This is in contrast to acyl complexes of the later transition metals where d orbitals, being capable of interacting with acyl $\pi^*_{CO}$, are usually low in energy and are occupied by electrons, thereby pushing $\pi^*_{CO}$ *up*. The higher positioning of the $\pi^*_{CO}$ level weakens the electrophilic nature of the acyl carbon. Therefore, the observed reactivity of $\eta^2$-acyl complexes is attained only when acyl ligands are bound to electron-deficient early-transition metal (and actinide) fragments, namely $d^0$ $Cp_2MX$.

Then can we say that the $\eta^2$-coordinate-acyl ligands in $Cp_2M(acyl)X$ complexes have "carbene" character, as has often been invoked? We must first clarify what "carbene" character means. Obviously there is a similarity between an $\eta^2$-coordinated acyl and a carbene in that both contain a low-lying LUMO, **30** vs. **31**, the large component of which is a carbon $p_\pi$. However, resonance form **4b** is somewhat misleading, because it might lead to an expectation that "carbene-type" behavior would also manifest itself in an elongated C=O bond. The experimental observations available so far argue against this expectation. No visible C=O elongation was observed in the X-ray structures of $Cp_2Ti(COCH_3)Cl$ (1.18 Å), $Cp_2Zr(COCH_3)(CH_3)$ (1.211 Å), and $Cp^*_2Th[COCH_2C(CH_3)_3]Cl$ (1.18 Å). Indeed the calculated C=O overlap populations, $P$(C=O), tell us that the C=O bond of an $\eta^2$ acyl is as strong as that of an $\eta^1$ acyl. This bond even gets slightly stronger on going from $\eta^1$ to $\eta^2$, e.g., for $Cp_2Ti(COCH_3)Cl$, $P$(C=O, $\eta^1$ O-outside) = 1.005, $P$(C=O, $\eta^2$ O-outside) = 1.029, and $P$(C=O, $\eta^2$ O-inside) = 1.028. The trend is what one would expect from our bonding picture presented in an earlier section. Coordination of acyl in an $\eta^2$ manner takes electrons out of a C–O antibonding orbital through the $n_-$–$d_\pi$ interaction, **10**, (and $n_-$–f interactions as well as in the actinide case, **11**).[37] On the other hand, there is no filled metal orbital available to transfer electrons back to the empty $\pi^*_{CO}$ orbital of acyl.

Since the so-called "carbene-type" reactivity may be accounted for by the low-energy position of $\pi^*_{CO}$, the ensuing electrophilicity and the positive charge of the acyl carbon, without the C=O elongation implied by **4b**, perhaps it would be more appropriate to describe the reactivity of the $\eta^2$ acyls as "carbenium-type".

Table I. Extended Hückel Parameters

| orbital | $H_{ii}$, eV | exponents[a] $\zeta_1$ | $\zeta_2$ |
|---|---|---|---|
| Ti 4s | −8.97 | 1.075 | |
| Ti 4p | −5.44 | 0.675 | |
| Ti 3d | −10.81 | 4.550 (0.4206) | 1.40 (0.7839) |
| Mn 4s | −8.63 | 1.8 | |
| Mn 4p | −5.06 | 1.8 | |
| Mn 3d | −11.59 | 5.15 (0.5311) | 1.90 (0.6479) |
| Zr 5s | −9.87 | 1.817 | |
| Zr 5p | −6.76 | 1.776 | |
| Zr 4d | −11.18 | 3.835 (0.6211) | 1.505 (0.5796) |
| U 7s | −5.50 | 1.914 | |
| U 7p | −5.50 | 1.914 | |
| U 6d | −5.09 | 2.581 (0.7608) | 1.207 (0.4126) |
| U 5f | −9.01 | 4.943 (0.7844) | 2.106 (0.3908) |
| U 6p | −30.03 | 4.033 | |
| C 2s | −21.4 | 1.625 | |
| C 2p | −11.4 | 1.625 | |
| O 2s | −32.3 | 2.275 | |
| O 2p | −14.8 | 2.275 | |
| Cl 3s | −30.0 | 2.033 | |
| Cl 3p | −15.0 | 2.033 | |
| H 1s | −13.6 | 1.30 | |

[a] Slater-type orbital exponents. The numbers of parentheses are coefficients used in the double-$\zeta$ expansion.

**Acknowledgment.** We are grateful to the National Science Foundation (R.H.) and the Deutsche Forschungsgemeinschaft and the Fonds der Chemischen Industrie (P.H., P.S.) for their support of this reason. Informative discussions with Drs. G. Erker and T. J. Marks were also of much value to us.

## Appendix

The calculations were carried out using the extended Hückel method,[38] with parameters as listed in Table I. Exponents for the Ti and Mn orbitals are from the works of Richardson et al.[39] and of Summerville and Hoffmann,[40] respectively. For Zr the exponents are those given by Basch and Gray.[41] Metal $H_{ii}$'s for Ti[42] and Mn[43] were taken from other work, while those for Zr were determined by charge iterative calculations on $Cp_2Zr(\eta^1\text{-}CH_2PPh_2)Cl$.[23] The U parameters are taken from previous work,[44] while those for C, O, Cl, and H are standard ones. A modified Wolfsberg–Helmholz formula[45] for $H_{ij}$ was used throughout the calculations.

Assumed geometries not listed in the text are as follows: $Cp_2Ti(COCH_3)Cl$: Ti–C(Cp), 2.388 Å; Ti–C(acyl), 2.07 Å; Ti–Cl, 2.49 Å; C–O, 1.18 Å; C–C(acyl), 1.47 Å, C–H(acyl), 1.09 Å; C–C(Cp), 1.42 Å; C–H, 1.09 Å; Cp–Ti–Cp, 132°; O–C–C-

(36) Note in this connection the M–O–M angles in $[Cp_2Zr(CH_3)]_2O$ and related compounds, which fall in the range of 169–180°: Hunter, W. E.; Hrncir, D. C.; Vann Bynum, R.; Penttila; R. A.; Atwood, J. L. *Organometallics* **1983**, *2*, 750–755, and references therein.

(37) The $n_+$–$d_\pi$ interaction weakens the acyl C–O bond, but this effect is cancelled out by the stronger $n_-$–$d_\pi$ interaction.

(38) (a) Hoffmann, R. *J. Chem. Phys.* **1963**, *39*, 1397–1412. (b) Hoffmann, R.; Lipscomb, W. N. *Ibid.* **1962**, *36*, 2179–2189. (c) Summerville, R.; Hoffmann, R. *J. Am. Chem. Soc.* **1976**, *98*, 7240–7254.

(39) Richardson, J. W.; Nieuwpoort, W. C.; Powell, R. R.; Edgell, W. E. *J. Chem. Phys.* **1962**, *36*, 1057–1061.

(40) Summerville, R. H.; Hoffmann, R. *J. Am. Chem. Soc.* **1976**, *98*, 7240–7254.

(41) Basch, H.; Gray, H. B. *Theor. Chim. Acta* **1966**, *4*, 367–376.

(42) Lauher, J. W.; Hoffmann, R. *J. Am. Chem. Soc.* **1976**, *98*, 1729–1742.

(43) Berke, H.; Hoffmann, R. *J. Am. Chem. Soc.* **1978**, *100*, 7224–7236.

(44) (a) Tatsumi, K.; Hoffmann, R. *Inorg. Chem.* **1980**, *19*, 2656–2658; **1984**, *23*, 1633–1634. (b) Tatsumi, K.; Nakamura, A. *J. Organomet. Chem.* **1984**, *272*, 141–154. (c) Cramer, R. E.; Mori, A. L.; Maynard, R. B.; Gilje, J. W.; Tatsumi, K. Nakamura, A. *J. Am. Chem. Soc.* **1984**, *106*, 5920–5926.

(45) Ammeter, J. H.; Bürgi, H.-B.; Thibeault, J. C.; Hoffmann, R. *J. Am. Chem. Soc.* **1978**, *100*, 3686–3692.

(acyl), 126°. $Mn(CO)_5(COCH_3)$: MnC(CO), 1.82 Å; C-O(CO), 1.14 Å; Mn-C(acyl), 2.07 Å; C-O(acyl), 1.21 Å; C-C(acyl), 1.51 Å; C-H, 1.09 Å; O-C-C(acyl), 115°. $Cp_2Zr(COCH_3)(CH_3)$: Zr-C(Cp), 2.5 Å; Zr-C($CH_3$), 2.336 Å; Zr-C(acyl), 2.197 Å; C-O, 1.211 Å; C-C(acyl), 1.492 Å; C-H($CH_3$), 1.1 Å; C-H(Cp), 1.08 Å; C-C(Cp), 1.40 Å; Cp-Zr-Cp, 130°; O-C-C(acyl), 120°. $Cp_2U(COCH_3)Cl$: U-C(Cp), 2.804 Å; U-C(acyl), 2.44 Å; U-Cl, 2.67 Å; C-O, 1.18 Å C-C(acyl), 1.47 Å; C-C(Cp), 1.42 Å; C-H, 1.09 Å; Cp-U-Cp, 138°; O-C-C(acyl), 118°.

**Registry No.** $Cp_2Zr(CH_3)_2$, 12636-72-5; $Cp_2U(CH_3)_2^{2+}$, 87136-09-2; $Cp_2Ti(COCH_3)Cl$, 66320-88-5; $Cp_2U(COCH_3)Cl^{2+}$, 96729-30-5; $Mn(CO)_5(COCH_3)$, 13963-91-2; $Cp^*_2Th[COCH_2C(CH_3)_3]Cl$, 74587-36-3; $[Mn(CO)_4(COCH_3)(COPh)]^-$, 55318-15-5; $Cp_2TiCl^+$, 96729-31-6; $Cp_2Zr(COCH_3)(CH_3)$, 60970-97-0; CO, 630-08-0.

# Why the Energetic Minimum Aluminum Vinylidene Is Not Observed in Low-Temperature Aluminum + Acetylene Reactions

**Andrew C. Scheiner and Henry F. Schaefer III***

*Contribution from the Department of Chemistry and Lawrence Berkeley Laboratory, University of California, Berkeley, California 94720.* *Received June 4, 1984*

**Abstract:** Ab initio molecular electronic structure theory has been used to investigate the Al + $C_2H_2$ potential energy surface. Particular emphasis was placed on resolving the apparent conflict between theory and experiment by examining the barrier to rearrangement between *cis*-AlHCCH (observed by ESR at 4 K) and $AlCCH_2$ (theoretically predicted global energy minimum). Analytic SCF gradients were employed with a double-$\zeta$ basis set to locate and characterize stationary points on the energy surface. Single point CI calculations using a double-$\zeta$ + polarization basis set have been carried out at the DZ-SCF stationary points. A DZP-CI barrier of 39.1 kcal for the *cis*-AlHCCH → $AlCCH_2$ isomerization has been found. Such a barrier is clearly prohibitive to this isomerization under the experimental conditions of 4 K. By comparing this isomerization to the bare HCCH → $CCH_2$ isomerization, the effect of the aluminum atom has been found to be significant.

The synthesis of the aluminum atom-acetylene adduct which was first reported by Kasai, McLeod, and Watanabe[1] and the more recent ESR analysis of this adduct by Kasai[2] suggest strongly the formation of a $\sigma$-bonded vinyl structure, **3**. Kasai's second paper[2] also discusses a trans → cis (**3** → **2**) conversion of this $\sigma$-bonded complex brought about by photoirradiation. A perhaps surprising feature is that no evidence was found to indicate the formation of the vinylidene complex, **1**, which has been predicted theoretically to be the global minimum on the Al-$C_2H_2$ energy surface.[3]

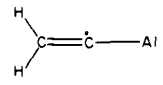

1

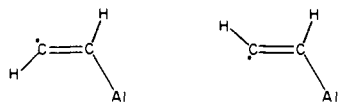

2 3

The purpose of the present research was twofold: first, to re-examine the vinylidene complex and the cis and trans (to the aluminum atom) $\sigma$-bonded vinyl radicals (structures **1**, **2**, and **3**, respectively) with analytic gradient techniques;[4] and second, to investigate the barrier to **2** → **1** rearrangement. As speculated in the previous theoretical study,[3] the presence of a large barrier to rearrangement would prohibit the formation of the low-energy vinylidene structure at the liquid helium temperatures of the ESR experiments.[1,2]

**Table I.** Calculated DZ-SCF Harmonic Vibrational Frequencies (in $cm^{-1}$) for $AlCCH_2$ (**1**), *cis*-AlHCCH (**2**), and *trans*-AlHCCH (**3**) and the **2** → **1** Transition State[a]

| $AlCCH_2$ | | *cis*-AlHCCH | | *trans*-AlHCCH | |
|---|---|---|---|---|---|
| 3360 | $CH_2$ a stretch | 3369 | $\nu_{C_\beta-H_\beta}$ | 3388 | $\nu_{C_\beta-H_\beta}$ |
| 3272 | $CH_2$ s stretch | 3238 | $\nu_{C_\alpha-H_\alpha}$ | 3210 | $\nu_{C_\alpha-H_\alpha}$ |
| 1796 | $\nu_{C-C}$ | 1671 | $\nu_{C-C}$ | 1664 | $\nu_{C-C}$ |
| 1543 | $CH_2$ scissors | 1286 | $\delta_{Al-C_\alpha-H_\alpha}$ | 1270 | $\delta_{Al-C_\alpha-H_\alpha}$ |
| 1109 | $CH_2$ wag | 1019 | $\tau_{H-C-C-H}$ | 993 | $\tau_{H-C-C-H}$ |
| 1048 | $CH_2$ rock | 973 | $\delta_{H-C-C-H}$ | 928 | $\delta_{H-C-C-H}$ |
| 520 | $\nu_{Al-C}$ | 568 | $\nu_{Al-C}$ | 571 | $\nu_{Al-C}$ |
| 239 | $\tau_{Al-C_\alpha-C_\beta}$ | 565 | $\tau_{Al-C_\alpha-C_\beta-H_\beta}$ | 522 | $\tau_{Al-C_\alpha-C_\beta-H_\beta}$ |
| 183 | $\delta_{Al-C_\alpha-C_\beta}$ | 212 | $\delta_{Al-C_\alpha-C_\beta}$ | 192 | $\delta_{Al-C_\alpha-C_\beta}$ |

| *cis*-AlHCCH → $AlCCH_2$ transition state | | *cis*-AlHCCH → $AlCCH_2$ transition state | |
|---|---|---|---|
| 3346 | $\nu_{C_\beta-H_\beta}$ | 513 | $\nu_{Al-C}$ |
| 3058i | $\nu_{C_\beta-H_\alpha} - \nu_{C_\alpha-H_\alpha}$ | 276 | $\tau_{Al-C_\alpha-C_\beta-H_\alpha}$ |
| 2383 | $\nu_{C_\beta-H_\alpha} + \nu_{C_\alpha-H_\alpha}$ | 258 | $\delta_{Al-C_\alpha-C_\beta-H_\beta}$ |
| 1805 | $\nu_{C-C}$ | 237 | $\tau_{Al-C_\alpha-C_\beta-H_\beta}$ |
| 927 | $\delta_{C_\alpha-C_\beta-H_\beta}$ | | |

[a] The carbon center bonded to aluminum is designated $C_\alpha$ and the hydrogen bonded to this carbon is designated $H_\alpha$. The remaining carbon and hydrogen are designated $C_\beta$ and $H_\beta$ respectively.

## Method

All geometries were precisely optimized by using self-consistent-field (SCF) analytic gradients.[4] The contracted double-$\zeta$ (DZ) basis set of Dunning and Hay,[5] designated Al(11s 7p/6s 4p), C(9s 5p/4s 2p), and H(4s/2s), was employed for these optimizations. A series of calculations based on finite nuclear displacements from the optimized DZ-SCF geometries were carried out to obtain harmonic vibrational frequencies for all stationary points. With use of the DZ-SCF structures, single point calculations with a DZ + polarization (DZ+P) basis set and including configuration interaction (CI) were also carried out. The polarization

(1) Kasai, P. H.; McLeod, D., Jr.; Watanabe, T. *J. Am. Chem. Soc.* **1977**, *99*, 3521.
(2) Kasai, P. H. *J. Am. Chem. Soc.* **1982**, *104*, 1164.
(3) Trenary, M.; Casida, M. E.; Brooks, B. R.; Schaefer, H. F. *J. Am. Chem. Soc.* **1979**, *101*, 1638.
(4) Osamura, Y.; Yamaguchi, Y.; Saxe, P.; Vincent, M. A.; Gaw, J. F.; Schaefer, H. F. *Chem. Phys.* **1982**, *72*, 131.
(5) Dunning, T. H.; Hay, P. J. "Modern Theoretical Chemistry"; Schaefer, H. F., Ed.; Plenum Press: New York, 1977; Vol. 3, pp 1-27.

0002-7863/85/1507-4451$01.50/0 